DOI: 10.1002/chem.200800376

Magnetic Endohedral Transition-Metal-Doped Semiconducting-Nanoclusters

Jon M. Matxain,* Elena Formoso, Jose M. Mercero, Mario Piris, Xabier Lopez, and Jesus M. Ugalde[a]

Abstract: Endohedral first-row transition-metal-doped TM@Zn_iS_i nanoclusters, in which TM stands for the first-row transition-metals from Sc to Zn, and $i=12$, 16, have been characterized. In these structures the dopant metals are trapped inside spheroidal hollow semiconducting nanoclusters. It is observed that some of the transition metals are trapped in the center of mass of the cluster, whereas others are found to be displaced from that center, leading to structures in which the transition metals display a complex dynamical behavior upon encapsulation. This fact was confirmed by quantum molecular dynamics calculations, which further confirmed the thermal stability of endohedral compounds. In the endohedrally-doped nanoclusters in which the transition-metal atom sits on the center of mass, the host hollow cluster structure remains undistorted after dopant encapsulation. Conversely, if the encapsulated transition-metal atom is displaced from the center of mass, the host hollow cluster structure suffers a very tiny distortion. Additionally, it is found that there is negligible charge transfer between the dopant transition-metal atom and its hollow cluster host and, after encapsulation, the spin densities remain localized on the transition-metal atom. This allows for the atomic-like behavior of the trapped transition-metal atom, which gives rise to their atomic-like magnetic properties. The encapsulation free energies are negative, suggesting that these compounds are thermodynamically stable.

Keywords: ab initio calculations · endohedral compounds · inorganic fullerenes · semiconducting nanoclusters · transition metals

Introduction

The properties of nanoparticles and nanoclusters differ with respect to those of their corresponding bulk material. However, as their bulk counterparts, nanoclusters can also be doped and, consequently, their properties be modified at will.[1]

Among nanocluster structural motifs, interest in hollow spherical structures has increased since the discovery of carbon buckminsterfullerenes.[2] These carbon clusters are able to build up molecular solids, in which each unit keeps its structure, similar to that of our isolated cluster.[3]

The electronic properties of these fullerenes and the solids made of them, fullerites, may be altered by the introduction of dopants, thereby yielding new materials with tailored properties. Fullerenes have been doped in three different ways: i) By substituting one or several carbon atoms by other similar atoms, such as B, N, or Si to yield the so called heterofullerenes, first produced by Smalley's group[4] in 1991; ii) Exohedrally, compounds in which atoms are placed outside the fullerene cages. It has been found that by exohedral doping a number of fullerites can be altered from the non-doped insulator to semiconductors,[5] or even high-temperature superconductors;[6,7] iii) Endohedrally, whereby atoms or molecules are trapped inside the fullerenes. The earliest one, La@C_{60}, was discovered by Heath et al. in 1985,[8] and after that many others have been found and their electronic structures explained.[9–13] Remarkably, no transition-metal atoms have been found encapsulated inside fullerenes.[14]

Boron nitride (BN) clusters are the ones next most widely studied hollow nanoclusters, owing to the fact that the BN unit is isoelectronic to C_2. A large amount of BN fullerenes, such as B_iN_i, $i=12,15,24,28$–60, have been investigated both theoretically and experimentally.[15–26]

[a] Dr. J. M. Matxain, Dr. E. Formoso, Dr. J. M. Mercero, Dr. M. Piris, Dr. X. Lopez, Prof. Dr. J. M. Ugalde
Kimika Fakultatea, Euskal Herriko Unibertsitatea
and Donostia International Physics Center (DIPC)
P.K. 1072, 20080 Donostia, Euskadi (Spain)
Fax: (+34)943015270
E-mail: jonmattin.matxain@ehu.es

Interestingly, the smallest synthesized BN fullerene, $B_{12}N_{12}$, has been seen to form stable solids, in which the structure of the cluster is not substantially altered. Namely, the structure of the boron nitride E-phase, discovered by Batsanov et al. in 1965,[27] and recently explained by Pokropivny to be a solid built by $B_{12}N_{12}$ fullerenes.[28] Other covalent crystals based on $B_{12}N_{12}$ fullerenes have been also characterized recently.[29,30]

Hollow nanoclusters of elemental metals have also been synthesized. For instance, experimental evidence of "free-standing" hollow clusters consisting of gold atoms, Au_{16-18}^-,[31] and lead atoms, Pb_{12}^{2-},[32] have recently been reported. As these gold cages have an average diameter larger than 5.5 Å, it was hypothesized that they could easily accommodate a guest atom inside. Indeed, this was further experimentally confirmed by Wang et al.,[33] who were able to isolate in the gas phase $Cu@Au_{16}$ and $Cu@Au_{17}$ nanoclusters. Similarly, the so called stannaspherene cluster, Sn_{12}^{2-} has also been characterized,[34] as a hollow cluster with icosahedral I_h symmetry and large enough diameter (>6 Å) as to encapsulate atoms inside. In particular, $TM@Sn_{12}^-$ (TM stands for transition metal) compounds have been found to be stable even in the gas phase, for most transition metals.[35] These endohedral clusters attain their stability by substantial charge transfer from the encapsulated atom to the cage Sn_{12}, which is an unsaturated cluster that gets stabilized by two additional electrons. Additionally, the $Mn@Sn_{12}$ endohedral compound has been characterized,[36] as an interesting high-spin endohedral transition-metal-doped nanocluster.

In addition to the C, BN, and metallic hollow nanoclusters mentioned above, binary hollow nanoclusters of semiconductor elements, such as II–VI elements, have also been investigated.[37–45] However, studies of the properties of endohedral compounds made of these hollow nanoclusters are scarce. Of particular relevance to the present research are the recent studies on the $Mn@Zn_{12}O_{12}$ endohedral compound,[46] and on the endohedral compounds of the type $(X@Zn_iO_i)_{i=4-16}^{0,\pm1}$, in which X is either an alkali metal or a halogen.[30]

The aim of this work is to study the endohedral first-row transition metals $(TM@Zn_iS_i)_{i=12,16}$. Endohedral transition-metal compounds are interesting, owing to their magnetic properties, which may lead to dimers with (anti)ferromagnetic coupling.[36]

We have considered trapped first row transition metals within $Zn_{12}S_{12}$ and $Zn_{16}S_{16}$ nanoclusters. The structures of these hollow Zn_iS_i nanoclusters have been characterized in previous works.[38,41] These two semiconducting nanoclusters have been chosen because of their high symmetry and highly spheroidal shape, which allow for favored endohedral structures as compared to other nanoclusters,[30] rather than for their experimentally proven enhanced stability.

Experimental evidence of the stability of Zn_iS_i, Cd_iS_i and Cd_iSe_i nanocluters was provided by Kasuya et al.,[47] who found that, in paticular, $Cd_{33}Se_{33}$ and $Cd_{34}Se_{34}$ are extermely stable in solution.

Additional evidence has recently been provided by Bel-Bruno and coworkers,[44,45] who found a number of stable Zn_iS_i nanoclusters in the gas phase.

Computational Details

All geometries have been fully optimized by using the gradient corrected hybrid B3LYP[48–50] functional within the Kohn–Sham implementation[51] of density functional theory.[52] Harmonic vibrational frequencies are determined by analytical differentiation of gradients, in order to determine whether the structures found are true minima or not, and to extract zero-point energies and vibrational contributions to Gibbs free energy, ΔG, which is reported at room temperature. The relativistic compact effective core potentials and shared-exponent basis set[53] of Stevens et al. (SKBJ) has been used for Zn and S, as described in the study of the isolated clusters,[41] and the fully relativistic multielectron-fit pseudopotentials, with 10 electrons in the core, developed by Dolg et al., were used for the trapped atoms.[54,55] Note that pure angular momentum functions were used throughout this study. To check for the reliability of this methodology, we have calculated the energy difference between high-spin and low-spin states of all first row TM, calculated as $\Delta E = E_{LS} - E_{HS}$, and are given in Table 1. Our calculations predict correctly the electronic state of the ground states, with energy differences which correlate correctly with the experimental ones. All the geometry optimizations and frequency calculations were carried out with the GAUSSIAN03 package.[56]

Table 1. Experimental and theoretical ΔE, the energy difference between the high (HS) and low spin (LS) states, of the first row transition-metal atoms, calculated as $E_{HS} - E_{LS}$.

Atom		ΔE_{Exp} [kcal mol^{-1}]	ΔE_{Theor} [kcal mol^{-1}]
Sc	^4F–^2D	−32.94	−24.44
Ti	^5F–^3F	−18.68	−13.93
V	^6D–^4F	−6.04	−5.98
Cr	^7S–^5S	21.71	19.47
Mn	^6S–^4D	66.61	52.55
Fe	^5D–^3F	34.24	29.18
Co	^4F–^2F	21.27	12.87
Ni	^3F–^1D	9.75	3.60

To further explore the thermal stability of these compounds, we also undertook ab initio thermal MD simulations at 298 K on some selected cases, controlled by means of the Nose thermostat as implemented in the SIESTA code,[57] within a DFT approach. Exchange and correlation effects were described using the generalized gradient approximation (GGA), within the revised Perdew–Burke–Ernzerhof (rPBE) functional.[58–60] Core electrons were replaced by Troullier–Martins norm-conserving pseudopotentials[61] in the Kleinman–Bylander factorized form.[62] Within the context of SIESTA, the use of pseudopotentials imposes basis orbitals adapted to them. Furthermore, SIESTA employs a localized basis set to represent the Kohn–Sham orbitals for valence electrons. Accordingly, the basis set of atomic orbitals is constructed from numerical solutions of the atomic pseudopotential, and are constrained to be zero beyond a cutoff radius. We used one basis set of double-ζ plus polarization quality (DZP). The single parameter (orbital energy shift) that defines the confinement radii of different orbitals was $\Delta E_{PAO} = 150$ meV, which gives typical precision within the accuracy of the used GGA functional. With this basis set, SIESTA calculates the self-consistent potential on a grid in real space. The fineness of this grid is determined in terms of an energy cutoff in analogy to the energy cutoff when the basis set involves plane waves. In our calculations, we used an equivalent plane wave cutoff energy of 200 Ry. These simulations were carried out for 5 ps with a chosen time step of 1 fs.

Results and Discussion

In this section the characterized first-row transition-metal endohedrally-doped nanoclusters, TM@$Zn_{12}S_{12}$ and TM@$Zn_{16}S_{16}$, are shown and their properties discussed. For each TM, the two lowest-lying spin states have been considered. In Table 2, the geometrical properties, such as the symmetry group of the endohedral compounds, the distance of the TM with respect to the center of the nanoclusters, R, and the r_{cavity} of the cluster are given, in Å, along with electronic properties such as the charge (q) and spin density (ρ_S) of the encapsulated transition metal. Energies like the energy difference between the high and low spin complexes (ΔE) and the encapsulation energy (ΔG_{enc}), in kcal mol^{-1}, are also given in Table 2, and will be compared to the energy differences observed for isolated transition-metal atoms.

A quick glance to the geometrical values given in Table 2 reveals that two types of stable endohedral compounds have been found. On the one hand, compounds in which the transition-metal atom is placed in the center of the cluster, $R=0$, and on the other hand, compounds where the transition-metal atom is displaced from the center of the cluster, $R>0$. These structures are depicted in Figure 1. Recall that the isolated $Zn_{12}S_{12}$ and $Zn_{16}S_{16}$ belong to the D_{2h} and D_{2d} symmetry groups and have r_{cavity} 2.54 and 3.14 Å, respectively, with standard deviations of 0 and 0.02. This indicates that these two nanoclusters are spherical.[30]

Comparing the r_{cavity} and standard deviations of the calculated endohedrally-doped compounds with respect to the isolated nanoclusters, it is observed that the nanoclusters do not get distorted appreciably upon encapsulation, an indication that the interaction between the host and the guest is small. Indeed, the small atomic charge of the trapped transition-metal atom, along with the fact that the spin densities are localized on the trapped atom, confirm that the charge

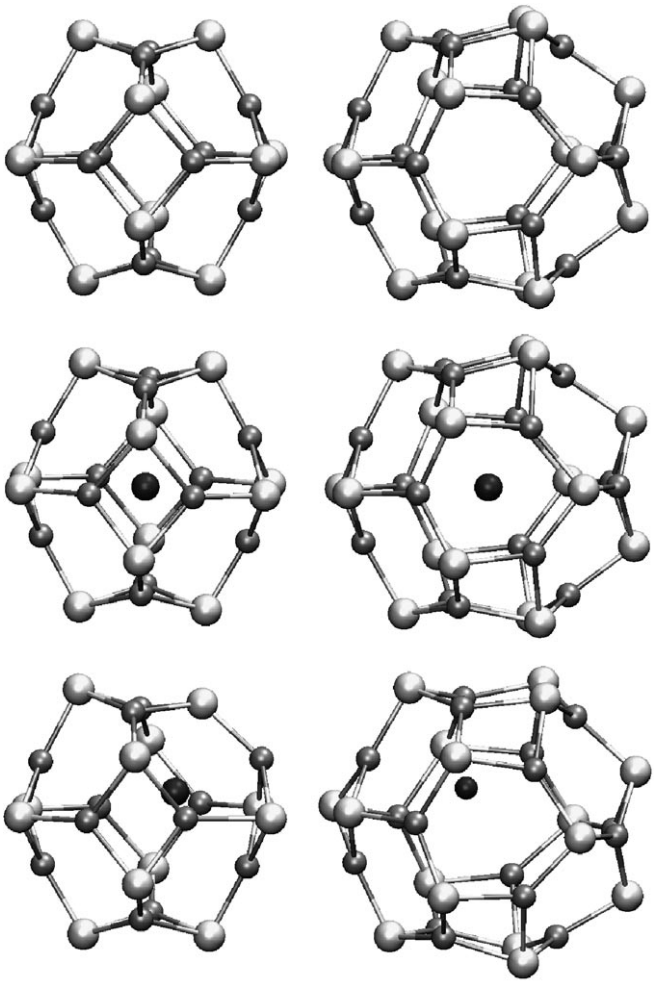

Figure 1. The structures of the isolated (top row) nanoclusters and stable endohedrally-doped TM@$Zn_{12}S_{12}$ (left column) and TM@$Zn_{16}S_{16}$ (right column) $R=0$ and $R>0$ nanoclusters.

Table 2. The distance of the TM with respect to the center of the nanocluster, and r_{cavity} [Å], with the standard deviation in parenthesis. Symm stands for the symmetry group of each structure. q is the atomic charge of the TM and, ρ_S its spin density. Finally, ΔE is the relative energy of the low-spin state with respect to the high-spin state, and ΔG_{enc} is the free energy of encapsulation, both are in kcal mol^{-1}.

		$Zn_{12}S_{12}$							$Zn_{16}S_{16}$						
		R	r_{cavity}	Symm	q	ρ_S	ΔE	ΔG_{enc}	R	r_{cavity}	Symm	q	ρ_S	ΔE	ΔG_{enc}
Sc	^2D	–	–	–	–	–	–	–	0	3.09 (0.03)	D_{2d}	0.44	0.87	–	−2.47
Sc	^4F	–	–	–	–	–	–	–	–	–	–	–	–	–	–
Ti	^3F	–	–	–	–	–	–	–	0	3.08 (0.04)	D_{2d}	0.38	1.86	8.82	−8.38
Ti	^5F	0.90	2.54 (0.13)	C_S	0.18	3.17	–	−17.54	1.54	3.09 (0.06)	C_1	0.02	3.49	–	−21.14
V	^4F	1.03	2.53 (0.18)	C_1	0.20	2.91	7.24	−7.41	0	3.09 (0.03)	D_{2d}	0.34	2.86	20.60	3.63
V	^6D	0.72	2.53 (0.07)	C_S	0.28	4.46	–	−15.63	1.21	3.09 (0.07)	C_S	0.12	4.61	–	−17.95
Cr	^5S	0	2.51 (0.00)	D_{2h}	0.49	3.94	14.81	−14.71	1.25	3.09 (0.09)	C_1	0.08	3.94	15.80	−16.57
Cr	^7S	0	2.52 (0.00)	D_{2h}	0.38	5.53	–	−10.04	0.83	3.09 (0.03)	C_1	0.22	5.61	–	−12.90
Mn	^4D	1.10	2.53 (0.09)	C_1	0.17	3.16	24.41	−21.21	1.66	3.09 (0.07)	C_1	0.05	3.35	30.05	−25.10
Mn	^6S	0	2.53 (0.00)	D_{2h}	0.44	4.65	–	6.93	0	3.09 (0.03)	D_{2d}	0.22	4.80	–	−2.60
Fe	^3F	1.04	2.52 (0.07)	C_1	0.17	2.23	6.44	−26.62	1.47	3.09 (0.06)	C_1	0.09	2.27	6.75	−26.28
Fe	^5D	0	2.51 (0.00)	D_{2h}	0.34	3.60	–	−3.87	0	3.09 (0.03)	D_{2d}	0.19	3.85	–	−3.85
Co	^2F	0.82	2.52 (0.05)	C_{2v}	−0.09	1.25	8.55	−15.38	1.44	3.09 (0.04)	C_S	0.04	2.69	−3.85	−20.35
Co	^4F	1.06	2.52 (0.05)	C_1	0.15	2.70	–	−11.06	0	3.09 (0.03)	D_{2d}	0.16	2.90	–	−3.63
Ni	^1D	–	–	–	–	–	–	–	1.84	3.10 (0.07)	C_S	−0.03	–	0.44	−17.47
Ni	^3F	0.75	2.52 (0.02)	C_{2v}	0.21	1.64	–	−14.36	1.46	3.09 (0.05)	C_S	0.05	1.71	–	−14.30
Cu	^2S	0.71	2.52 (0.02)	C_1	0.25	0.66	–	−13.12	1.50	3.09 (0.04)	C_S	0.01	0.70	–	−15.03
Zn	^1S	0	2.54 (0.00)	D_{2h}	0.20	–	–	5.98	0	3.09 (0.02)	D_{2d}	0.09	0.00	–	−2.14

and spin transfers from the TM to the nanocluster are negligible.

This allows us to draw a schematical picture of these endohedral structures as a neutral transition-metal atom inside a neutral nanocluster, with the spin density localized on the transition-metal atom, for both $R=0$ and $R>0$ compounds.

The relative high-spin and low-spin energies shown in Table 2 reveal that endohedral transition-metal-doped nanoclusters favor high-spin states, with the sole exception of $Co@Zn_{16}S_{16}$, for which its low-spin state is 3.85 kcal mol^{-1} more stable than its high-spin state.

Additionally, as shown in Table 2, we observe that the encapsulation free energies are negative, which means that the formation of these endohedral compounds is thermodynamically allowed. There are three exceptions, however, $Mn(^6S)@Zn_{12}S_{12}$, $Zn(^1S)@Zn_{12}S_{12}$ and $V(^4F)@Zn_{16}S_{16}$, have positive encapsulation energies. In Table 2 notice that the Sc atom, both in its doublet or quartet state, the Ti atom in its triplet state and the Ni atom in the singlet state do not form stable endohedral structures inside $Zn_{12}S_{12}$. Let us discuss in more detail the results obtained for $R=0$ and $R>0$ compounds.

Structural properties: The middle transition-metal elements are found to remain stable at the center of the $Zn_{12}S_{12}$ nanocluster. Namely, $TM@Zn_{12}S_{12}$, with TM = Cr (^5S, ^7S), Mn (^6S), Fe (^5D) are stable structures. For the $Zn_{16}S_{16}$, both the early and middle transition-metal elements are found to remain stable at the center of the nanocluster, i.e.: $TM@Zn_{16}S_{16}$, with TM = Sc (^2D), Ti (^3F), V (^4F), Mn (^6S), Fe (^5D), Co (^4F) are stable structures. Finally, the late transition-metal endohedral nanoclusters of Ni and Cu have the metal displaced from the center of the nanocluster, whereas Zn favors a centered position inside both $Zn_{12}S_{12}$ and $Zn_{16}S_{16}$ clusters. The endohedral nanoclusters with $R>0$, in which the metal is forced to be at the center of the clusters, are high order stationary points that have several vibrational modes with a negative force constant. Both types of structural families, namely, $R=0$ and $R>0$, are depicted in Figure 1, along with their corresponding isolated nanostructures.

Observe that transition-metal elements that can be trapped at the center of the $Zn_{12}S_{12}$ nanocluster have high-spin state. Conversely, for the $Zn_{16}S_{16}$ nanocluster, the earlier transition-metal elements have low-spin, whereas the middle transition-metal elements have high-spin state. Thus the highest spin state corresponds to the $Cr@Zn_{12}S_{12}$ endohedral nanocluster, which is predicted to posses large atomic-like magnetism and carry a magnetic moment of 6 μ_B.

A study of the r_{cavity} values of these compounds reveals that they differ slightly from the 2.54 (0.00) and 3.14 (0.02) Å values of the isolated $Zn_{12}S_{12}$ and $Zn_{16}S_{16}$ cavities.[30] In addition, the symmetry groups of these endohedral structures are the same as those of the isolated nanoclusters, which means that the nanoclusters are not geometrically altered upon transition-metal encapsulation.

Focusing on the geometrical properties of the endohedrally-doped nanoclusters with the metal-displaced off-center, $R>0$ structures, it is observed that the displacement of the metal leads to a loss of symmetry of the structures, as a consequence of the distortion on the hollow cluster structure upon the encapsulation of the transition metal. Recall, nevertheless, the small values of the standard deviation and how similar are the radii of the cavities as compared to the radii of the corresponding nanoclusters with the transition-metal atom placed at the center. Notice, finally, that the value of R in $TM@Zn_{16}S_{16}$ endohedral nanoclusters is larger than in $TM@Zn_{12}S_{12}$, as one could expect owing to the larger cavity radius of the former.

For $R=0$ compounds the charge of the transition-metal atom decreases as it moves towards the right in the periodic table. Thus, for $TM@Zn_{12}S_{12}$ nanoclusters, the transition-metal atomic charge decreases from the 0.49 e of Cr (^5S) nanocluster to 0.20 e of the Zn (^1S) nanocluster. Additionally, in the $TM@Zn_{16}S_{16}$ case this decrease occurs from the 0.44 e of Sc (^2D) to the 0.09 e of Zn (^1S). The electron density cloud of the transition-metal atom gets more compact as one moves to the right in the periodic table, hence, the charge transfer from the transition-metal atom to the nanocluster decreases.

For off-center endohedral nanoclusters, $R>0$ structures, the atomic charge of the transition metal fluctuates very little between a minimum charge transfer of 0.12 e in $V(^6D)@Zn_{16}S_{16}$ and a maximum of 0.28 e for $V(^6D)@Zn_{12}S_{12}$. The calculated spin densities for both $R=0$ and $R>0$ families reveal that the spin is mainly located on the trapped transition-metal atom.

Consequently, we may conclude that in these endohedral compounds both the transition metal and the nanocluster maintain their isolated structure. This was not the case of the endohedral $X@Zn_iS_i$ nanoclusters, in which X stands for alkali metal and halogens. For the former an electron was transferred from the alkali metal atom to the nanocluster and for the latter and electron was transferred from the nanocluster to the halogen atom.[30]

Energies: In this subsection the relative energies, ΔE, between of the low-spin (LS) states with respect to their corresponding high-spin state (HS) and the encapsulation free energies, ΔG_{enc}, for the dopant transition-metal atom to be encapsulated inside the $(ZnS_i)_{i=12,16}$, shown in Table 2, are discussed. The ΔG_{enc} for a given endohedral cluster is calculated with respect to the isolated cluster and the transition-metal atom with the same spin multiplicity as the endohedral complex.

The calculated ΔE values suggest that the high-spin states of the endohedral nanoclusters are lower in energy than their low-spin states, irrespective of whether the transition-metal atom is trapped at the center or off-center. The only exception to this rule is $Co@Zn_{16}S_{16}$. Observe that the calculated spin densities, shown in Table 2, are very supportive of the almost pure spin localization at the metal center. However, a word of caution is due here, concerning the inaccur-

ateness of the hybrid approximated functionals to treat "localized" spin systems.[63]

Recall that for the isolated transition-metal atoms the high spin states are favored with respect to their low-spin states, except for Sc, Ti, and V, which have the low-spin ground states (See Table 1). The energy differences of the Mn nanoclusters peak at 24.41 and 30.05 kcal mol^{-1} for Mn@$Zn_{12}S_{12}$ and Mn@$Zn_{16}S_{16}$, respectively. Then, the energy difference decreases as one moves from Mn towards either end, the left or the right, of the periodic table. Additionally, the ΔE values of the endohedral nanoclusters are smaller than those of isolated transition-metal atoms, indicating a higher relative stabilization of the excited states of the transition-metal atoms upon encapsulation. This higher relative stabilization is remarkable for Ti, V, and Co endohedral nanoclusters, since the excited state of the isolated atom becomes now the ground state in the endohedral nanocluster.

The negative values of ΔG_{enc} show that most of these endohedral transition-metal-doped nanoclusters are thermodynamically stable. Note that ΔG_{enc} are more negative for those spin states that are excited states in the corresponding isolated metal atoms. This means that these states are stabilized more in the endohedral structures, in agreement with the calculated ΔE_s. In general, the most exergonic compounds are those of low-spin middle transition-metal nanoclusters, irrespective of whether the trapped transition-metal atoms in on the center or off-center. Thus, the most exergonic endohedral nanoclusters are those of Fe(^3F), with values around -26 kcal mol^{-1}. In general, the ΔG_{enc} are slightly more negative in TM@$Zn_{16}S_{16}$ than in TM@$Zn_{12}S_{12}$ nanoclusters by ≈ -2 kcal mol^{-1}. This is an indication that TM@$Zn_{16}S_{16}$ nanoclusters are somewhat more stable than their corresponding TM@$Zn_{12}S_{12}$ nanoclusters.

Quantum dynamics of the trapped atom: Ab initio molecular dynamics simulations have been carried out for two selected cases, Zn(^1S)@$Zn_{12}S_{12}$ and Ti(^5F)@$Zn_{12}S_{12}$, as representatives of the endohedral nanoclusters with the trapped dopant atom at the center and off-center, respectively. We have set a simulation time of 5 ps, with a time step of 1 fs, and the trajectories have been calculated at a constant average temperature of 298 K. Figure 2 shows how the energies of these nanoclusters vary during the simulation.

It can be observed, from the Figure 2, that the energies of both nanoclusters oscillate around the same value over the whole simulation period. A fact which is very supportive of the thermal stability of the endohedral nanostructures. Therefore, these endohedral structures are predicted to be stable enough to survive long time at room temperature as to allow for their experimental characterization.

The distances of the trapped transition metal with respect to the center of mass of the Zn(^1S)@$Zn_{12}S_{12}$ and Ti(^5F)@$Zn_{12}S_{12}$ endohedral nanoclusters during the simulation time are depicted in Figure 3. Recall that in the optimum structure of Zn(^1S)@$Zn_{12}S_{12}$, the endohedral dopant Zn atom is at the center, $R=0$, of the nanocluster. Conversely, in the

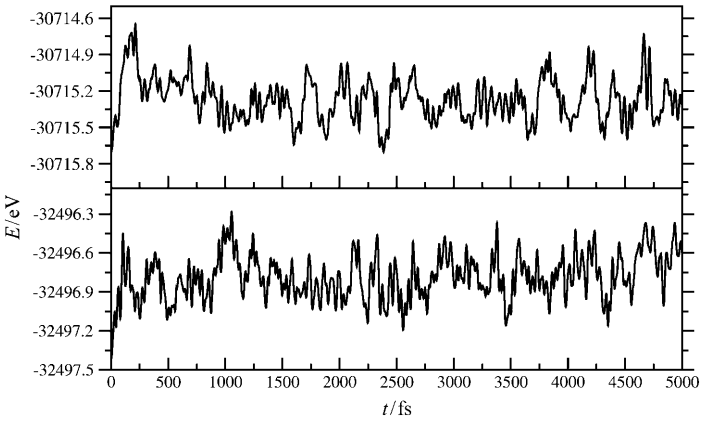

Figure 2. Variation of the energy, in eV, of Ti(^5F)@$Zn_{12}S_{12}$ (top panel) and Zn(^1S)@$Zn_{12}S_{12}$ (bottom panel) endohedral nanoclusters as a function of time.

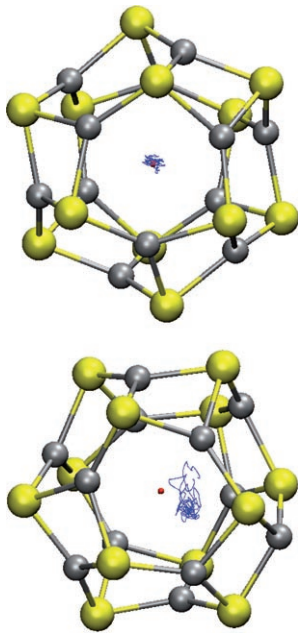

Figure 3. Variation of the distance, R, in Å, of the trapped transition-metal atom from the center of mass of the nanocluster as a function of time. Ti@$Zn_{12}S_{12}$ (——) and Zn@$Zn_{12}S_{12}$ (-----).

optimum structure of Ti(^5F)@$Zn_{12}S_{12}$, the titanium atom is at $R=0.90$ Å.

In the case of Zn(^1S)@$Zn_{12}S_{12}$, the quantum molecular dynamics calculations show that the Zn moves around the nanocluster's center, up to a maximum radial distance of 0.4 Å. The average radial separation of the endohedral Zn atom being 0.18 ± 0.07 Å. The dynamical trajectory of the Zn atom inside $Zn_{12}S_{12}$ is outlined in Figure 4. It is observed that the Zn atom remains confined at the center of the nanocluster.

However, the dynamical behavior of the trapped titanium atom in the Ti(^5F)@$Zn_{12}S_{12}$ is very different. Our calculations show that Ti localizes in one off-center grove, which

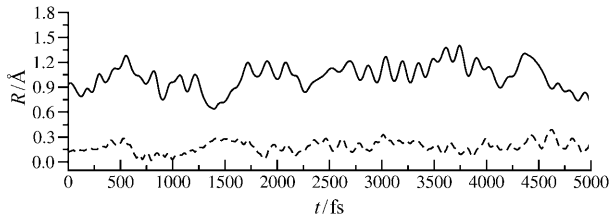

Figure 4. Dynamical trajectories of the transition-metal atom inside the nanocluster. Top $Zn(^1S)@Zn_{12}S_{12}$ and bottom for $Ti(^5F)@Zn_{12}S_{12}$. The plots were prepared as follows. For each saved structure along the dynamics, the center of mass of the spheroid was set on the origin (red dot), and the coordinates of all atoms in the system referred to this center of mass. Then, the average position for each of the atoms of the spheroid along the dynamics was calculated and the corresponding average spheroid structure is the one shown in the figure. Finally, the blue line corresponds to the positions of the inner atom (Zn or Ti) with respect to the center of mass of the spheroid for each saved structure.

expands radially from 0.7 to 1.3 Å from the center. The average radial distance of the titanium within such grove has been calculated to be 1.03 ± 0.16 Å, a radial distance very similar to the $R = 0.90$ Å obtained for the optimum minimum structure. Observe that there are four equivalent such groves for the trapped titanium atom in the $Ti@Zn_{12}S_{12}$ nanoclusters. We have observed no passing from one such grove to another during our simulation time. This is indicative that such groves are separated by energy barriers larger than kT.

One can envisage two main paths connecting the above mentioned groves. One passing through the center of mass of the nanocluster and another one along a "constant" radius path. The former will denoted as the radial path and the latter as the angular path. We have been able to optimize the structures that correspond to the highest energy point on each path and, consequently, this allows us to estimate the barrier heights of the two paths. We have collected these barrier heights in Table 3.

Table 3. Estimated energy barries, in kcal mol^{-1}, connecting the various confinement groves of the endohedral nanoclusters which have the trapped transition-metal atom indicated in first column, displaced from the center of the nanocluster. ΔE^{+}_{rad}, stands for the barrier along the path connecting the groves through the center of mass of the nanocluster and ΔE^{+}_{ang} is the barrier along the lateral path.

		$Zn_{12}S_{12}$		$Zn_{16}S_{16}$	
	$2S+1$	ΔE^{+}_{rad}	ΔE^{+}_{ang}	ΔE^{+}_{rad}	ΔE^{+}_{ang}
Ti	5	9.84	1.77	12.47	9.90
V	4	12.67	1.32	–	–
V	6	4.46	3.60	9.44	5.96
Cr	5	–	–	8.73	7.13
Cr	7	–	–	5.50	2.01
Mn	4	9.49	2.51		
Fe	3	9.18	2.32	12.18	1.39
Co	2	19.34	0.00	6.67	10.31
Co	4	6.59	4.04	–	–
Ni	1	–	–	42.59	15.13
Ni	3	2.89	0.00	7.86	0.82
Cu	2	3.38	0.05	8.95	7.71

Observe that most barriers lie well above kT for $T = 298$ K, namely, ≈ 0.6 kcal mol^{-1}. Consequently, the trapped atom will not jump from grove to grove, as shown by our quantum molecular dynamic calculations, for it has not enough energy as to surmount the energy barrier. Finally, it is worth noting that in spite of the predicted "weak" host-guest interaction, our calculations demonstrate that for a number of these $TM@Zn_iS_i$ nanoclusters, it turs out to be large enough as to raise barriers, larger than kT, which prevent off-center trapped transition metals to cross the nanocluster's center.

Conclusions

In this work the endohedrally-doped $TM@Zn_iS_i$ nanoclusters have been characterized. TM stands for the first-row transition-metals from Sc to Zn, and $i = 12,16$. Two type of structures have been observed. On the one hand structures where the dopant transition-metal atom is placed at the center of the nanoclusters, denoted as $R = 0$ and, on the other hand, nanoclusters where the dopant transition-metal atom is displaced from the center to a distance R, denoted as $R > 0$ structures. In all these structures the transition-metal atom causes a small or negligible distortion on the nanocluster upon encapsulation. The small atomic charge of the trapped transition-metal atom, along with the fact that the spin densities are localized on the metal atom, reveal that in most cases there is little charge and spin transfer from the transition-metal atom to the nanocluster. This is indicative of a weak guest–host interaction.

The calculated relative energies of the low-spin states with respect to their corresponding high-spin states, ΔE, reveal that the high-spin doped nanoclusters are more stable than the low-spin ones, irrespective of whether the trapped atom lies on the center of mass of the cluster or displaced off-center.

The encapsulation free energies, ΔG_{enc}, are found to be negative. This means that the formation of these endohedral compounds is thermodynamically allowed. The ΔG_{enc} encapsulation free energies of the trapped excited states of the transition-metal atoms are more negative than those of their corresponding ground states. This indicates a higher relative stabilization of the excited states of the transition-metal atom upon encapsulation.

Quantum molecular dynamics calculations carried out on these endohedrally-doped nanoclusters are very supportive of the thermal stability of the characterized structures. Those with optimum geometries having the trapped transition atom at the center of mass of the nanocluster, present a deep enough confinement well as to retain the dopant atom around its equilibrium position. Structures where the optimum geometry shows the dopant trapped transition-metal atom displaced from the center of mass, have a number of symmetry dictated confinement groves for the transition-metal atom. The calculated energy barriers of the angular and the radial paths, connecting the various groves of the

off-center trapped endohedral nanoclusters, suggest that, at room temperature, the transition metal will not move from grove to grove.

Our calculations indicate that the $(Zn_iS_i)_{i=12,16}$ clusters act as a host protecting the spins of the trapped dopant transition-metal atom, giving rise to the atomic magnetism. It is well-known that the local properties of a dopant transition-metal atom strongly depend on their vicinal environment. For these particular endohedral nanoclusters, the interaction between the trapped dopant transition-metal atoms and the $(Zn_iS_i)_{i=12,16}$ hosts is weak, allowing them to behave atomic-like and keep their spin states unaltered.

Continued experimental and theoretical studies of similar doped nanoclusters may lead to the discovery of new families molecular magnets with tunable magnetic properties.

Acknowledgements

This research was funded by Eusko Jaurlaritza (the Basque Government) SAIOTEK program, and the Spanish Ministerio de Educacion y Ciencia. The SGI/IZO-SGIker UPV/EHU (supported by Fondo Social Europeo and MCyT) is gratefully acknowledged for generous allocation of computational resources.

[1] G. Cantele, E . Degoli, E. Luppi, R. Magri, D. Ninno, G. Iadonisi, S. Ossicini, *Phys. Rev. B* **2005**, *72*, 113303.
[2] H. W. Kroto, H. R. Heath, S. C. O'Brien, R. F. Curl, R. E. Smalley, *Nature* **1985**, *318*, 162.
[3] B. L. Zhang, C. Z. Wang, K. M. Ho, C. T. Chan, *Europhys. Lett.* **1994**, *28*, 219.
[4] T. Guo, C. Jin, R. E. Smalley, *J. Phys. Chem.* **1991**, *95*, 4948.
[5] M. Freemantle, *Chem. Eng. News* **1999**, *77*, 15.
[6] S. C. Erwin, M. R. Pederson, *Phys. Rev. Lett.* **1991**, *67*, 1610.
[7] Y. Iwasa, H. Hayashi, T. Furudate, T. Mitani, *J. Am. Chem. Soc.* **1996**, *118*, 14960.
[8] J. R. Heath, S. C. O'Brien, Q. Zheng, Y. Liu, R. F. Curl, H. W. Kroto, F. K. Tittel, R. E. Smalley, *J. Am. Chem. Soc.* **1985**, *107*, 7779.
[9] S. Erkoç, L. Turker, *THEOCHEM* **2003**, *634*, 195.
[10] M. S. Dresselhaus, G. Dresselhaus, and P. C. Eklund; Academic Press, San Diego, **1996**.
[11] C. M. Cardona, B. Elliott, L. Echegoyen, *J. Am. Chem. Soc.* **2006**, *128*, 6480.
[12] T. Weiske, D. K. Böhme, J. Hru ák, W. Krätschmer, H. Schwarz, *Angew. Chem.* **1991**, *103*, 898; *Angew. Chem. Int. Ed. Engl.* **1991**, *30*, 884.
[13] A. Krapp, G. Frenking, *Chem. Eur. J.* **2007**, *13*, 8256.
[14] J. Cioslowski, *Electronic Structure Calculations on Fullerenes and Their Derivatives*; Oxford University Press, New York, **1995**.
[15] T. Oku, A. Nishiwaki, I. Narita, *Phys. B* **2004**, *531*, 184.
[16] J. M. Matxain, J. M. Ugalde, M. D. Towler, R. J. Needs, *J. Phys. Chem. A* **2003**, *107*, 10004.
[17] T. Oku, A. Nishiwaki, I. Narita, *Sol. Stat. Commun.* **2004**, *130*, 171.
[18] T. Oku, A. Nishiwaki, I. Narita, M. Gonda, *Chem. Phys. Lett.* **2003**, *380*, 620.
[19] J. O. Jensen, D. R. Yarkony, *Chem. Phys. Lett.* **1987**, *141*, 391.
[20] F. Jensen, H. Toftlund, *Chem. Phys. Lett.* **1993**, *201*, 89.
[21] G. Seifert, P. W. Fowler, D. Mitchell, D. Porezag, Th. Frauenheim, *Chem. Phys. Lett.* **1997**, *268*, 252.
[22] D. L. Strout, *Chem. Phys. Lett.* **2004**, *383*, 95.
[23] S. S. Alexandre, M. S. C. Mazzoni, H. Chacham, *Appl. Phys. Lett.* **1999**, *75*, 61.
[24] T. Oku, A. Nishiwaki, I. Narita, *Sci. and Technol. of Adv. Mater.*, **2004**, page 1.
[25] H. S. Wu, X. H. Xu, F. Q. Zhang, H. Jiao, *J. Phys. Chem. A* **2003**, *107*, 6609.
[26] H. S. Wu, H. Jiao, *Chem. Phys. Lett.* **2004**, *386*, 369.
[27] S. S. Batsanov, G. E. Blohina, A. A. Deribas, *Zh. Strukt. Khim.* **1965**, *6*, 227.
[28] A. V. Pokropivny, *Diamond Relat. Mater.* **2006**, *15*, 1492.
[29] V. V. Pokropivny, A. V. Pokropivny, V. V. Skorokhod, A. V. Kurdyumov, *Dopov. Nats. Akad. Nauk Ukr.* **1999**, *4*, 112.
[30] J. M. Matxain, L. A. Eriksson, E. Formoso, M. Piris, J. M. Ugalde, *J. Phys. Chem. C* **2007**, *111*, 3560.
[31] S. Bulusu, X. Li, L. S. Wang, X. C. Zeng, *Proc. Natl. Acad. Sci. USA* **2006**, *103*, 8326.
[32] L. Cui, X. Huang, L. Wang, J. Li, L. Wang, *J. Phys. Chem. A* **2006**, *110*, 10169.
[33] L. Wang, S. Bulusu, H. Zhai, X. Zeng, L. Wang, *Angew. Chem.* **2007**, *119*, 2973; *Angew. Chem. Int. Ed.* **2007**, *46*, 2915.
[34] L. Cui, X. Huang, L. Wang, D. Zubarev, A. I. Boldyrev, J. Li, L. Wang, *J. Am. Chem. Soc.* **2006**, *128*, 8390.
[35] L. Cui, X. Huang, L. Wang, J. Li, L. Wang, *Angew. Chem. Int. Ed.* **2007**, *46*, 742.
[36] J. M. Matxain, M. Piris, E. Formoso, J. M. Mercero, X. Lopez, J. M. Ugalde, *ChemPhysChem* **2007**, *8*, 2096.
[37] S. Hamad, S. Cristol, C. R. A. Catlow, *J. Am. Chem. Soc.* **2005**, *127*, 9479.
[38] S. Hamad, C. R. A. Catlow, E. Spano, J. M. Matxain, J. M. Ugalde, *J. Phys. Chem. B* **2005**, *109*, 2703.
[39] J. M. Matxain, J. M. Mercero, J. E. Fowler, J. M. Ugalde, *J. Phys. Chem. A* **2003**, *107*, 9981.
[40] J. M. Matxain, J. M. Mercero, J. E. Fowler, J. M. Ugalde, *J. Phys. Chem. A* **2004**, *108*, 10502.
[41] J. M. Matxain, J. E. Fowler, J. M. Ugalde, *Phys. Rev. A* **2000**, *61*, 53201.
[42] J. M. Matxain, J. E. Fowler, J. M. Ugalde, *Phys. Rev. A* **2000**, *62*, 53201.
[43] J. M. Matxain, J. M. Mercero, J. E. Fowler, J. M. Ugalde, *Phys. Rev. A* **2001**, *64*, 53201.
[44] E. Sanville, A. Burnin, J. J. BelBruno, *J. Phys. Chem. A* **2006**, *110*, 2378.
[45] A. Burnin, E. Sanville, J. J. BelBruno, *J. Phys. Chem. A* **2005**, *109*, 5026.
[46] H. Liu, S. Wang, G. Zhou, J. Wu, W. Duan, *J. Chem. Phys.* **2006**, *124*, 174705.
[47] A. Kasuya, R. Sivamohan, Y. A. Barnakov, I. M. Dmitruk, T. Nirasawa, V. R. Romanyuk, V. Kumar, S. V. Mamykin, K. Tohji, B. Jeyadevan, K. Shinoda, T. Kudo, O. Terasaki, Z. Liu, R. V. Belosludov, V. Sundararajan, T. Kavazoe, *Nat. Mater.* **2004**, *3*, 99.
[48] A. D. Becke, *Phys. Rev. A* **1988**, *38*, 3098.
[49] A. D. Becke, *J. Chem. Phys.* **1993**, *98*, 1372.
[50] C. Lee, W. Yang, R. G. Parr, *Phys. Rev. B* **1988**, *37*, 785.
[51] W. Kohn, L. J. Sham, *Phys. Rev.* **1965**, *140*, A1133.
[52] P. Hohenberg, W. Kohn, *Phys. Rev.* **1964**, *136*, B864.
[53] W. J. Stevens, M. Krauss, H. Basch, P. G. Jasien, *Can. J. Chem.* **1992**, *70*, 612.
[54] M. Dolg, U. Wedig, H. Stoll, H. Preuss, *J. Chem. Phys.* **1987**, *86*, 866.
[55] J. M. L. Martin, A. Sundermann, *J. Chem. Phys.* **2001**, *114*, 3408.
[56] M. J. Frisch, G. W. Trucks, H. B. Schlegel, G. E. Scuseria, M. A. Robb, J. R. Cheeseman, J. A. Montgomery, Jr., T. Vreven, K. N. Kudin, J. C. Burant, J. M. Millam, S. S. Iyengar, J. Tomasi, V. Barone, B. Mennucci, M. Cossi, G. Scalmani, N. Rega, G. A. Petersson, H. Nakatsuji, M. Hada, M. Ehara, K. Toyota, R. Fukuda, J. Hasegawa, M. Ishida, T. Nakajima, Y. Honda, O. Kitao, H. Nakai, M. Klene, X. Li, J. E. Knox, H. P. Hratchian, J. B. Cross, V. Bakken, C. Adamo, J. Jaramillo, R. Gomperts, R. E. Stratmann, O. Yazyev, A. J. Austin, R. Cammi, C. Pomelli, J. W. Ochterski, P. Y. Ayala, K. Morokuma, G. A. Voth, P. Salvador, J. J. Dannenberg, V. G. Zakrzewski, S. Dapprich, A. D. Daniels, M. C. Strain, O. Farkas, D. K. Malick, A. D. Rabuck, K. Raghavachari, J. B. Foresman, J. V. Ortiz, Q. Cui, A. G. Baboul, S. Clifford, J. Cioslowski, B. B. Stefanov, G. Liu, A. Liashenko, P. Piskorz, I. Komaromi, R. L. Martin, D. J. Fox, T.

Keith, M. A. Al-Laham, C. Y. Peng, A. Nanayakkara, M. Challacombe, P. M. W. Gill, B. Johnson, W. Chen, M. W. Wong, C. Gonzalez, and J. A. Pople; Gaussian 03, Revision C.02, Gaussian, Inc., Wallingford, CT, **2004**.
[57] J. M. Soler, E. Artacho, J. D. Gale, A. Garcia, J. Junquera, P. Ordejon, D. Sanchez-Portal, *J. Phys. Condens. Matter* **2002**, *14*, 2745.
[58] J. P. Perdew, K. Burke, M. Ernzerhof, *Phys. Rev. Lett.* **1996**, *77*, 3865.
[59] Y. Zhang, W. Yang, *Phys. Rev. Lett.* **1998**, *80*, 890.
[60] B. Hammer, L. B. Hansen, J. K. Norskov, *Phys. Rev. B* **1999**, *59*, 7413.
[61] N. Troullier, J. L. Martins, *Phys. Rev. B* **1991**, *43*, 1993.
[62] L. Kleinman, D. M. Bylander, *Phys. Rev. Lett.* **1982**, *48*, 1425.
[63] J. M. Mercero, J. M. Matxain, X. Lopez, D. M. York, A. Largo, L. A. Eriksson, J. M. Ugalde, *Int. J. Mass Spectrom.* **2005**, *240*, 37.

Received: March 3, 2008
Published online: July 30, 2008

